ADVANCED HEALTHCARE MATERIALS
www.advhealthmat.de

Initial Formation of the Skin Layer of PLGA Microparticles

*Farrokh Sharifi, Andrew Otte, and Kinam Park**

The Special Issue Dedicated to Professor Nicholas Peppas

Poly(lactide-*co*-glycolide) (PLGA) has been extensively used in making long-acting injectable formulations. The critical factors affecting the PLGA formulation properties have been adjusted to control the drug release kinetics and obtain desirable properties of PLGA-based drug delivery systems. The PLGA microparticle formation begins as soon as the drug/PLGA-dissolved in the organic solvent phase (oil phase) is exposed to the water phase. The initial skin (or shell) formation on the oil droplets occurs very quickly, sometimes in the matter of milliseconds, and studying the process has been difficult. The skin formation on the PLGA emulsion droplet surface that can affect the subsequent hardening steps is examined. PLGA droplets with different compositions are prepared. Using collimated light and a high-speed camera made it possible to detect the diffusion of acetonitrile from the oil phase into the water phase during the oil droplet formation. Although the skin formation is not visible on the surface of the oil phase droplet with the current setup, the droplet shapes, solid strand formation, and the difference in the spreading time suggest that the initial contact time between the oil and water phases in the range of a few seconds is critical to the properties of the skin.

1. Introduction

Aliphatic polyesters have been widely used in biomedical, pharmaceutical, and agricultural applications for their excellent biodegradability and biocompatibility.[1] The common polyesters are poly(lactide-co-glycolide) (PLGA), polylactide (PLA), polyglycolide (PGA), poly(ϵ-caprolactone) (PCL), and poly(γ-valerolactone).[2] For example, PLA is used in applications requiring high mechanical strength and toughness, such as orthopedic devices, sutures, and interventional devices for cardiovascular diseases.[3,4] Additionally, copolymerization of the aliphatic polyesters has been used to change the properties of the polymers and make them suitable for the needed application. PLGA is an amorphous copolymer with tunable degradation rate, flexibility, and firmness.[5] PLGA has been used widely in biomedical and pharmaceutical areas, such as drug delivery,[6–11] tissue engineering, and regenerative medicine.[12,13]

Characterization of the diffusion, phase separation, gel formation, and quantification of the dynamics of phase inversion began with dark ground imaging techniques.[14] This visualization technique focused on the concentration gradient that occurred as water diffused into the polymer-organic solvent solution. Developing characterization methods of visualizing the precipitation kinetics of the skin layer formation allows preparing PLGA formulations more systematically than the trial and error approach. The skin formation of in situ implants has been extensively characterized, as the burst release is closely correlated to the kinetics of skin formation, where slow forming implants tend to have thicker skins resulting in slower drug release kinetics than faster forming implants.[14] The mobility of the drug is reduced in the nonphase inverted interior core, which is more viscous than through the highly porous, thin skin layer.[15]

The in situ gel-forming implants are orders of magnitude larger in size than microparticles. The gel-forming implants are formulated with water-miscible solvents (e.g., acetonitrile (ACN) and *N*-methyl-2-pyrrolidone), contrary to microparticles typically manufactured with solvents with much lower water solubility (e.g., dichloromethane and ethyl acetate (EA)). Thus, the precipitation kinetics varies drastically. Additionally, the in situ implants can be regarded as simple solutions or suspensions. Their manufacturability is mainly limited to the time and temperature of mixing, contrary to microparticles with many manufacturing processing steps that can be incorporated or varied. The solvent limitations imposed by in situ implants may offer microparticles an advantage in adjusting the drug loading and release profiles by controlling the formulation and manufacturing variables. In situ implants are advantageous in their simplicity as compared with microparticle formulations. Irrespective of PLGA formulations, the drug release is controlled by the initial PLGA precipitation upon contact with water.

1.1. PLGA Chemistry and Physicochemical Properties

The formation mechanisms of PLGA-based microparticles cannot be understood or controlled without a fundamental

F. Sharifi, A. Otte, K. Park
Weldon School of Biomedical Engineering
206 South Martin Jischke Drive, West Lafayette, IN 47907, USA
E-mail: kpark@purdue.edu
K. Park
Departments of Biomedical Engineering and Pharmaceutics
206 South Martin Jischke Drive, West Lafayette, IN 47907, USA

The ORCID identification number(s) for the author(s) of this article can be found under https://doi.org/10.1002/adhm.202101427

DOI: 10.1002/adhm.202101427

understanding of the chemistry and resultant molecular properties of PLGA. PLGA is a linear copolymer of two monomers, lactic acid (L) and glycolic acid (G), and the L:G ratio of widely used PLGAs ranges from 50:50 to 100:0 (i.e., poly(lactic acid)). PLGAs with ratios ranging from 0:100 (poly(glycolic acid)) to 50:50 are found to be only soluble in highly fluorinated solvents[16] due to their high crystallinity. Thus, they have not been used in drug delivery applications.

Most PLGAs used in drug delivery are random copolymers. The L:G ratio and molecular weight represent the intrinsic variables used to modify the behavior. Controlling the monomer sequence has been used as an additional way to tune the polymer properties.[17] Sequenced PLGAs ($(L\text{-}G)_n$) are known to degrade with a relatively linear molecular weight loss rather than the exponential decay shown with a random sequence.[18] This difference was mainly attributed to the nucleophilic attack by water, where the random sequence has a broader and more diverse range of reactivity rates with water. In contrast, the block sites have many G-G units that are likely to be cleaved more quickly than the G-L/L-G and the more hydrophobic L-L units.[17] Detailed PLGA characterization presents a unique opportunity to compare the qualitative and quantitative sameness of two different PLGAs.[19]

The molecular weight of PLGA polymers also needs to be considered when selecting a PLGA polymer. The molecular weights have been described with their inherent viscosity range instead of the molecular weights measured by gel permeation chromatography (GPC) or static light scattering for convenience. PLGA copolymerization is typically performed via a direct polycondensation reaction of lactic acid and glycolic acid[20,21] or ring-opening polymerization of the cyclic dimers, lactide and glycolide.[22–25] Ring-opening polymerization offers much higher control of polymerization.[26]

The PLGA molecule end group can further alter the overall properties.[27–29] While multiple end groups have been prepared, ester-terminated or free carboxylic acid end groups are typically used. The less hydrophilic nature of the ester-terminated end-group typically results in a reduced polymer degradation rate due to the lower hydrophilicity relative to the acid end-capped polymers.[30,31] The free acid end-group has been used to anchor ionized drugs, e.g., peptides, through salt formation.[32]

1.2. Microparticle Formation

The two traditional methods of PLGA microparticle formation include an oil-in-water (o/w) emulsion for encapsulating hydrophobic compounds and a water-in-oil-in-water (w/o/w) emulsion for hydrophilic compounds. The emulsion solvent evaporation technique is essentially a two-step process: emulsification of a polymeric solution/suspension followed by solvent extraction, evaporation, and polymer precipitation. During emulsification, the oil (or discontinuous) phase is broken up into smaller droplets through the shear stress by the homogenizer, mixer, sonicator, or another device. This emulsification step is the main processing parameter that determines the microparticle size distribution. Numerous reports demonstrate how manufacturing differences can impact the physicochemical properties of the microspheres and ultimately their performance,[33–36] illustrating the importance of the process and how incremental changes in processing variables can significantly influence the resultant microparticle properties.

1.3. Skin Formation

The first step toward microparticle formation is the initial, instantaneous solvent extraction, where nascent microparticles are formed. After removing a sufficient amount of solvent during this initial solvent extraction, a skin layer forms at the droplet interface.[37] This skin layer formation governs the solvent removal rate. The outermost layer dictates the compositional structure of the layers beneath: a dense, nonporous layer hinders solvent diffusion, whereas a porous layer presents minimal diffusional resistance.[38]

Multiple types of layered formations have been described in the phase separation and precipitation of asymmetric membranes, closely mimicking the surface of an oil droplet in contact with an extraction solution. Some examples of layered formation include: (i) a dense skin layer supported by a layer containing closed cell pores or pores in an open interconnected type; (ii) a thin skin layer with a typical structure of closely packed polymeric spheres, a so-called nodular structure with the nodule size of 20–100 nm supported by a highly open porous layer, often containing large elongated voids called "macrovoids"; and (iii) an interconnected pore structure with variation in pore size (0.1-1 μm) over the membrane thickness.[39] These macrovoids were first shown to be suppressed or eliminated through multiple mechanisms, most notably choosing a solvent–nonsolvent pair with a low tendency of mixing,[40] increasing the polymer concentration in the casting solution,[40,41] or addition of solvent to the extraction medium.[41] In general, macrovoid formation occurs under conditions that favor rapid precipitation, and void can be minimized by increasing the polymer solution's viscosity.

For solvents with low solubilities in water, the solvent–water demixing is slower due to decreased diffusional rates, leading to a slower skin layer formation with slower and lower quantities of water migration into the sublayers. This typically results in more homogeneous structures, particularly noticeable at the surface. Due to the low solvent solubility in the water phase, more water is required to cause local precipitation.

Temperature can significantly influence the skin layer through control of the precipitation rate. Bovine serum albumin microparticles formed through a w/o/w technique at high temperatures were shown to have a uniform internal pore distribution and a weak dense skin layer. In contrast, lower temperature preparation resulted in a thicker but porous skin layer and larger internal pores.[42] The temperature impacted both the encapsulation efficiency and the amount of surface-exposed protein on the microparticle. High temperatures (42 °C) increased the skin solidification rate, and lower temperatures (5–15 °C) inhibited mobility of the protein movement to the surface. Temperatures in between seem to allow enough protein migration to the surface and result in a significant initial burst.

A successful design of the microparticle-based system requires balancing the control among the phase inversion process dynamics, the resultant skin layer and core morphology, and the drug's physical state(s) in the polymer matrix. Each step is controlled or can be varied through multiple parameters. However, often the

Table 1. Formulation or processing parameters and respective mechanistic effect on the microparticles coupled with their expected performance impact.

Formulation or processing parameter change	Mechanistic effect of parameter change	Impact on encapsulation efficiency and drug release
PLGA L:G ratio increase	• Increase in hydrophobicity • Decrease in water absorption	Drug release rate decreases[43–47]
PLGA molecular weight (MW) increase	Low MW polymer more soluble in an organic phase → • Slow solidification resulting in porous microparticles • Degradation rate decrease	Drug release rate decreases[48–50]
Drug loading increase	Increase of drug:PLGA ratio	Drug release rate increases[10,51,52]
Polymer concentration increase	• Increase in viscosity delays drug diffusion from droplets • Polymer precipitates faster on surface	Encapsulation efficiency increases[53,54]
Emulsifier concentration increase	Decrease in particle size	Drug release rate increases[55,56]
Energy input increase (e.g., homogenization speed, sonication amplitude)	• Decrease in particle size • Increase in particle surface area	Drug release rate increases[57–59]
Discontinuous:continuous phase ratio decrease	Increase concentration gradient → Fast solidification	Encapsulation efficiency increased[53,60]
Extraction temperature increase	• Fast ramp → thin shell and large core • Gradual ramp → thick shell and medium core[61]	

parameters are interdependent, which is one of the highly complicated features of developing PLGA-based microparticle products.

1.4. Microparticle Hardening

From a mechanical standpoint, microparticle formation is, in essence, a continuum from skin formation. Once nascent microparticles are obtained, microparticle hardening continues through further solvent extraction. Depending on the final specifications and manufacturing process, this hardening in the initial extraction solution can be completed or sufficient for further handling.

As solvent extraction continues, the embryonic microparticles shrink to form localized, dense drug-PLGA microstructures throughout the microparticles. Simultaneously, water molecules diffuse in to replace solvent molecules. The spaces occupied by water and residual solvent become void after drying. As the extraction rate and hardening step are also controlled by temperature, the mobility of the polymer chains and the time spent in the rubbery phase are also influenced by the extraction temperature, leading to a potentially more dense polymeric matrix or phase segregation of the drug. After the desired amount of solvent has been extracted from the microparticles into the extraction phase, the hardened microparticles are collected and dried by freeze/vacuum drying.[36] **Table 1** summarizes a broad overview of typical formulation and processing variables that modify the encapsulation efficiency and drug release kinetics of small molecules, peptides, and proteins. The impacts of the formulation- and manufacturing-based parameters on the properties of the microparticles have been discussed in detail.[11]

Here, we studied droplet formation using different PLGA concentrations in two solvents, EA and ACN:EA mixture, injected into the water phase at three flow rates of 10, 100, and 200 µL min^{-1}. The collimated light and high-speed camera were used to increase the sensitivity of the imaging to the refractive index and detect the solvent diffusion from the oil phase during the droplet formation. Although the starting point of PLGA precipitation was not clear, our preliminary data indicate a correlation between the skin formation and spreading time of the oil phase at the surface of the static water phase.

2. Experimental Section

2.1. Materials

PLGA copolymer (ester end-capped), with the lactide:glycolide (L:G) ratio of 75:25, molecular weight of 180 kDa, and inherent viscosity (IV) of 0.8–1.2 dL g^{-1} was purchased from Lactel® Absorbable Polymers. EA and ACN were obtained from Fisher Scientific. Poly(vinyl alcohol) (PVA) 40–88 (molecular weight = 205 000 g mol^{-1}) was purchased from Millipore Sigma. Nile Red was obtained from Sigma Aldrich.

2.2. Formulation Information for the Organic and Aqueous Phases

This work focuses on the initial PLGA precipitation and skin formation on the surface of organic phase droplets. The organic phases were prepared using nine combinations by varying the PLGA concentration, 1%, 10%, 20%, and 30% (w/w), and the solvent type having different water solubilities, ACN (water soluble), EA (partially water soluble, 8.3 g 100 mL^{-1})[31], and ACN:EA (1:1 by volume). The formulations with partially water-soluble solvents, i.e., EA and ACN:EA, had relatively higher interfacial tensions between the two phases than the formulation made with PLGA/ACN. All the solvents were dyed using Nile Red with a concentration of 0.01% to visualize the oil phase. The water phase consisted of 1% (w/v) PVA, an emulsifier, in deionized water. Sample preparations and experiments were done at room temperature (20 °C). The PVA-dissolved water was sieved using 45 µm mesh (Dual Manufacturing), then filtered using a 5 µm syringe filter (Pall Laboratory) to remove dust particles originating

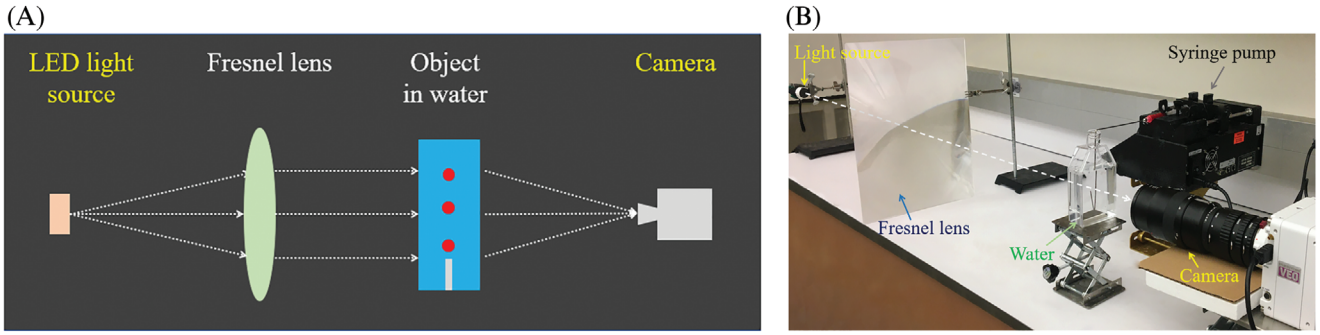

Figure 1. A schematic A and an experimental setup B used to generate oil phase droplets in a water bath to study the PLGAprecipitation over time with a high-speed camera and collimated light (focused shadowgraph).

from PVA powders. Brookfield DV2T viscometer with a cone and plate geometry was used to measure the viscosity of the oil phases at room temperature (20 °C).

2.3. Oil Phase Droplet Formation and Imaging

A 250 mL Falcon® cell culture flask (Corning) was used as a water bath because of its transparent, flat walls that improved the imaging quality of the oil droplet formation with minimal undesirable light reflections. The oil phases were injected into the water phase at three flow rates of 10, 100, and 200 µL min^{-1} using a syringe pump (Harvard Apparatus-PHD 2000). A 14-gauge needle with outer and inner diameters of 2.109 and 1.6 mm, respectively, was chosen to inject the oil phase into the water bath. Because the density of all the oil phase formulations was lower than the water phase, the injection needle was bent facing upwards to avoid attachment of the oil phase to the needle tip.

As described in Section 2.2, the oil phase was made with different PLGA concentrations. Therefore, the density and viscosity of the oil phase were not constant. Additionally, the oil phase was injected into the water phase with different flow rates. To have a better understanding of the interaction between the viscous and inertial forces and their effects on the shape and size of the oil phase droplets, the Reynolds number of the oil phase (Re_o) or dispersed phase was calculated using the equation below:[62]

$$Re_o = \frac{\rho_o u_0 d_i}{\mu_o} = \frac{\rho_o Q_0 d_i}{\mu_o A_i} \quad (1)$$

where ρ_o, u_0, Q_0, μ_o represent density, flow velocity, flow rate, and viscosity of the oil phase, and d_i and A_i are the inner diameter and cross-section area of the oil phase tube, respectively.

2.4. Shape of the Oil Phase Droplets and PLGA Precipitation

A high-speed camera (Phantom VEO 1310) with a 100 mm Zeiss lens and a set of extension tubes was used for imaging. Collimated light was generated using a LED light source with a diameter of 2 mm and a Fresnel lens (provided by Ametek, Inc.) to improve the contrast (**Figure 1**). In this method, fluids with different refractive indexes can be detected because the change in refractive index distorts the collimated light beam, which results in variation in the light intensity and, thus, detection by the camera. Additionally, the droplet generation was recorded under natural/ordinary (non-collimated) light for comparison. The exposure time was 1500 and 3000 µs when the collimated and natural lights were used, respectively. All the videos were recorded at 300 frames per second (fps). ImageJ software was used to measure the size of the droplets and the neck part of the oil phases during the thinning and pinching-off. The size of the droplets was measured when the droplets were 1.5 cm above the outlet of the oil phase injection tube.

2.5. Formation and Spreading Time of the Droplets

The formation time of the oil phase droplets was measured at the needle tip of the oil phase injection tube. After formation, the oil phase droplets rose until they reached the surface of the water phase due to the lower density of the oil phases compared to that of the water phase. Then, the droplets spread at the surface of the water phase because they were not rigid enough during the formation time and the surface tension of the water phase (72 mN m^{-1}) is higher than EA (23.75 mN m^{-1}) and ACN (29.25 mN m^{-1}).[63,64] The spreading time was measured from when the oil phase droplet touched the surface until it started to spread. For different oil phase formulations and flow rates, the time between two pinch-offs was measured from the time the previous droplet separated from the oil phase until the next droplet got to the pinch-off point.

2.6. Statistics

Data were presented as the mean ± SD. The sample size was 3 for the analysis ($n = 3$). One-sided ANOVA was used to verify statistically significant differences between sample means.

3. Results and Discussion

Different oil phase formulations with PLGA concentrations of 1%, 10%, 20%, and 30% and organic solvents of EA, a mixture of 1:1 EA:ACN, and ACN were injected into the water phase. As the oil phase was injected toward the outside of the needle, there was a pinch-off point where the connection between the feeding oil phase and the forming drop was broken up.[65] The pinch-off

Table 2. (A) Viscosity, density, and (B) Reynolds number of the oil phases made with different formulations, injected in the water phase bath with two flow rates of 100 and 200 µL min^{-1} at room temperature (20 °C). Data are reported as mean ± SD ($n = 3$).

(A)

PLGA concentration (%wt/wt)	EA solvent		ACN:EA solvents	
	Viscosity [mPa s]	Density [g mL^{-1}]	Viscosity [mPa s]	Density [g mL^{-1}]
1	0.51 ± 0.05	0.818 ± 0.003	0.23 ± 0.06	0.745 ± 0.012
10	27.07 ± 0.93	0.852 ± 0.005	14.46 ± 0.47	0.799 ± 0.009
20	641.8 ± 9.3	0.886 ± 0.002	196.3 ± 4.7	0.830 ± 0.005
30	8632 ± 186	0.909 ± 0.007	2153 ± 47	0.866 ± 0.002

(B)

PLGA concentration (%wt/wt)	EA solvent		ACN:EA solvents	
	Flow rate 100 µL min^{-1}	Flow rate 200 µL min^{-1}	Flow rate 100 µL min^{-1}	Flow rate 200 µL min^{-1}
1	2.128 ± 0.064	4.2567 ± 0.064	4.2982 ± 0.187	8.5964 ± 0.187
10	0.042 ± 0.005	0.0835 ± 0.005	0.0733 ± 0.019	0.1466 ± 0.019
20	0.0018 ± 0.0002	0.0037 ± 0.0002	0.0056 ± 0.0001	0.0112 ± 0.0001
30	0.0001 ± 0.00004	0.0003 ± 0.00004	0.0005 ± 0.00004	0.0011 ± 0.00004

point varied depending on the formulation and the flow rate of the oil phase.

Table 2A shows the viscosity and density values of the oil phases made at different PLGA concentrations in EA and ACN:EA. The viscosity of the oil phase exponentially increased with PLGA concentration with the rates of 0.59 $e^{0.332c}$ and 0.31 $e^{0.308c}$ when EA and ACN:EA were used, respectively, where c is the concentration of the PLGA in the oil phase in percent.

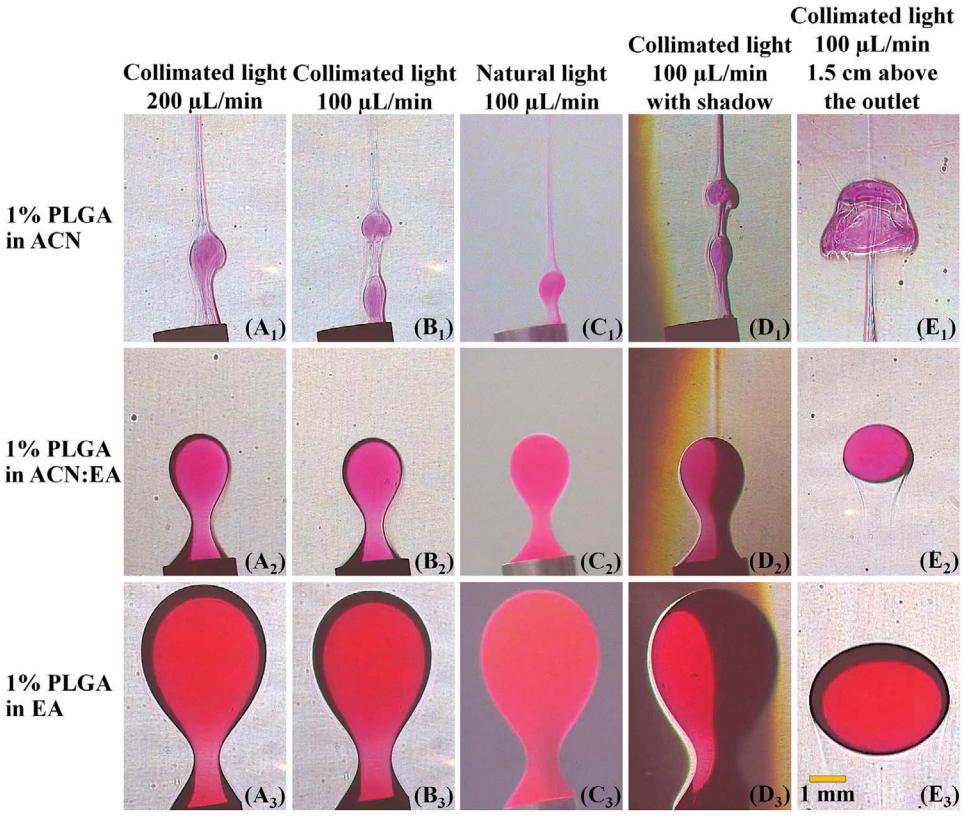

Figure 2. Oil phase droplet formation with 1% PLGA in different solvents. The images were taken 10 ms before the pinch-off. The scale bar: 1 mm for all the images.

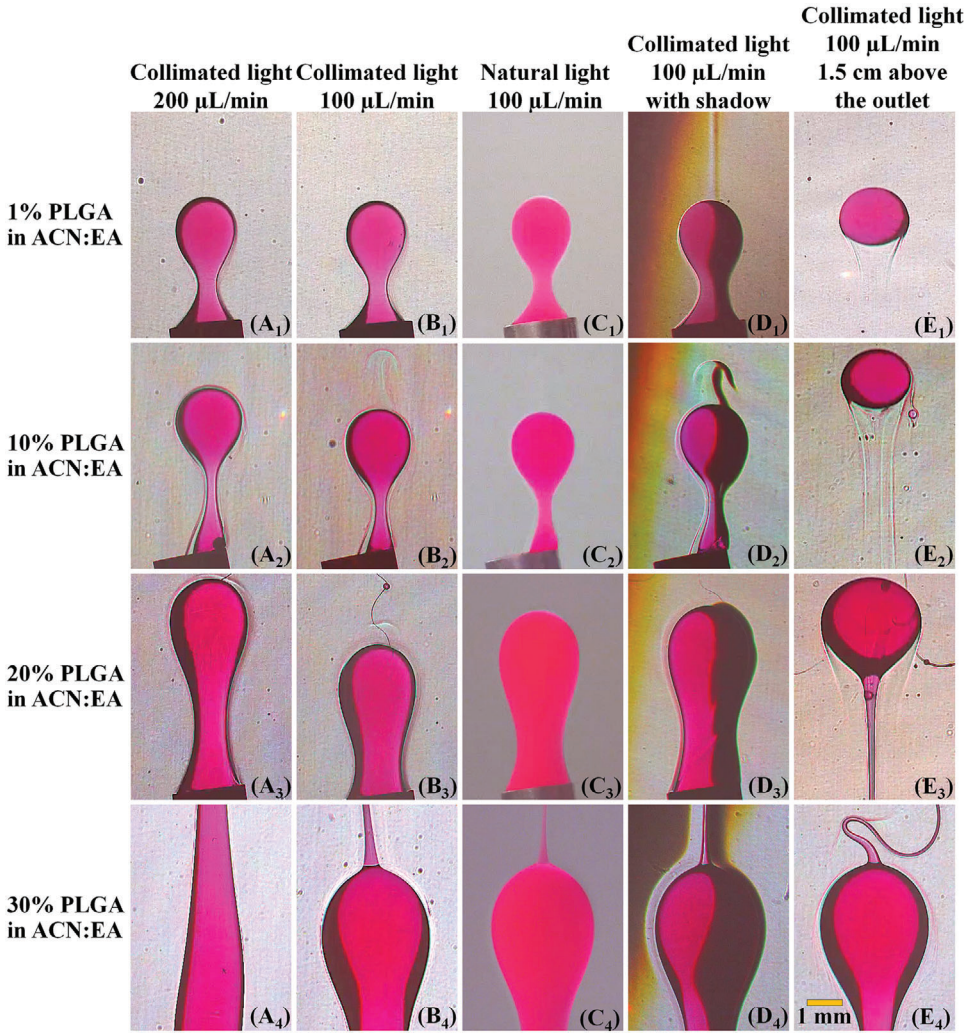

Figure 3. Oil phase droplet formation with the PLGA concentrations of 1% (A_1-E_1), 10% (A_2-E_2), 20% (A_3-E_3), and 30% (A_4-E_4) in ACN:EA solvent with the volume ratio of 1:1. The images were taken 10, 50, 1000, and 7000 ms before the pinch-off when the PLGA concentration was 1%, 10%, 20%, and 30%, respectively. The scale bar: 1 mm for all the images.

Additionally, to better understand the change of the inertial to viscous force ratios, the Reynolds number was calculated for different oil phase formulations at the injection flow rates of 100 and 200 µL min^{-1} (Table 2B). As shown in the table, all the experiments were conducted at a low Re number regime in the range of 0.0001–8.6, indicating the dominant effects of viscous force compared to the inertial force. By definition, there is a linear relationship between the Re number and the flow rate (Equation 1). However, when the PLGA concentration increased from 1% to 30% in both solvents (EA and ACN:EA), the Re number exponentially reduced due to the exponential increase of the viscosity of the organic phase by increasing the PLGA concentration.

Figure 2 shows the images of the oil phase droplets in the water phase 10 milliseconds (ms) before the pinch-off. The PLGA concentration was kept constant at 1% for all the formulations, and the solvents with different water solubility were used. Two flow rates of 100 and 200 µL min^{-1} were tested (Figure 2A,B). The imaging results with collimated and natural light were compared in Figure 2B,C. By changing the position of the light source parallel to the Fresnel lens, part of the LED light was cut off. This arrangement gave shadowgraph effects, which helped increase the contrast of the images (Figure 2B,D). The last column (Figure 2E) demonstrates the shape and size of the oil phase droplet 1.5 cm above the outlet of the needle. The figure shows no significant difference between the size and shape of the droplet when the flow rate was increased from 100 to 200 µL min^{-1}. This means that the viscous force dampened the effects of increased inertial force when the flow rate increased by 100 µL min^{-1} due to the low Re number regime and dominant effects of the viscous force (Table 2B). When only ACN was used, the separation of the ACN (with transparent color) from the oil phase (with red color) was visible.

By decreasing the water miscibility of the solvent, the size of the droplets became larger. When a solvent with higher water solubility was used, the solvent diffusion from the oil phase increased. Additionally, because the density of the ACN is lower than EA, 1% PLGA in ACN:EA (w/w) has a lower viscosity than 1% PLGA in EA. Therefore, the viscous force reduced when 1%

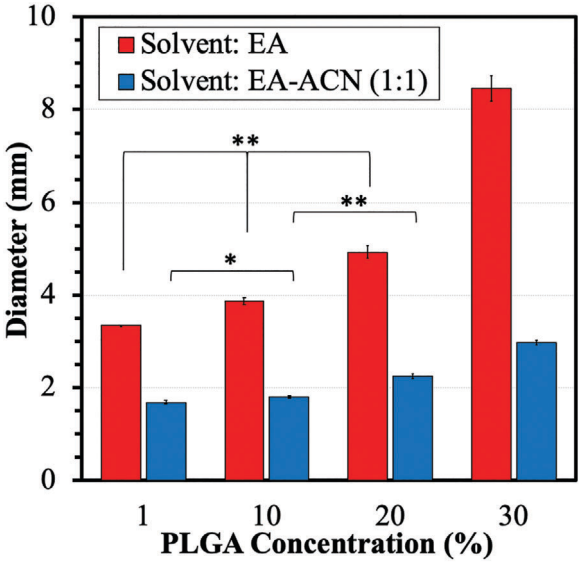

Figure 4. Size of the droplets made with the PLGA concentrations of 1–30% in EA and ACN:EA (1:1, v:v). Data are reported as mean ± SD ($n = 3$, $^{*}p < 0.05$; $^{**}p < 0.01$).

PLGA in ACN:EA was used, compared to 1% PLGA in EA. This increased Re number (Table 2B) and less resistance to the change created by the inertial force and, thus, the formation of smaller droplets.

The effects of the PLGA concentration in the organic solvent ACN:EA on the shape and size of the droplets were studied (**Figure 3**). Because the droplet formation rate decreased as the PLGA concentration increased (due to the enhanced viscous force), the images were taken at different times: 10, 50, 1000, and 7000 ms before the pinch-off when PLGA concentrations of 1%, 10%, 20%, and 30% were used, respectively. For example, when 30% PLGA was used, at 10 ms before the pinch-off, most droplets would not be visible at the needle outlet except a strand. The droplet size increased as the PLGA concentration was increased due to the increased amount of viscous force. Similarly, Figure S1 (Supporting Information) shows the oil phase droplets made of different PLGA concentrations in the range of 1–30% in EA and two flow rates of 100 to 200 µL min^{-1}.

Panels B_2 and D_2 of Figure 3 show the diffusion of the solvent, most likely ACN from the oil phase, into the water phase due to its higher solubility than EA. The diffusion of the ACN from the droplet before the pinch-off was visible. When the PLGA concentration was increased from 1% to above 20%, the droplets formed with strands at their top and bottom. The droplet formation at a higher PLGA concentration became slower due to the enhanced viscous force that resisted the deformation. Therefore, at the pinch-off point, the solvent had enough time to diffuse out of the oil phase, followed by PLGA precipitation as strands attached to the top and bottom of the droplets (Figure 3,E_3 and E_4). Besides strands, satellite and subsatellite drops were formed for all PLGA concentrations due to several breakup sequences around the neck part of a deformed filament.[66] The satellites separated from the oil phase droplets at low PLGA concentrations (1% and

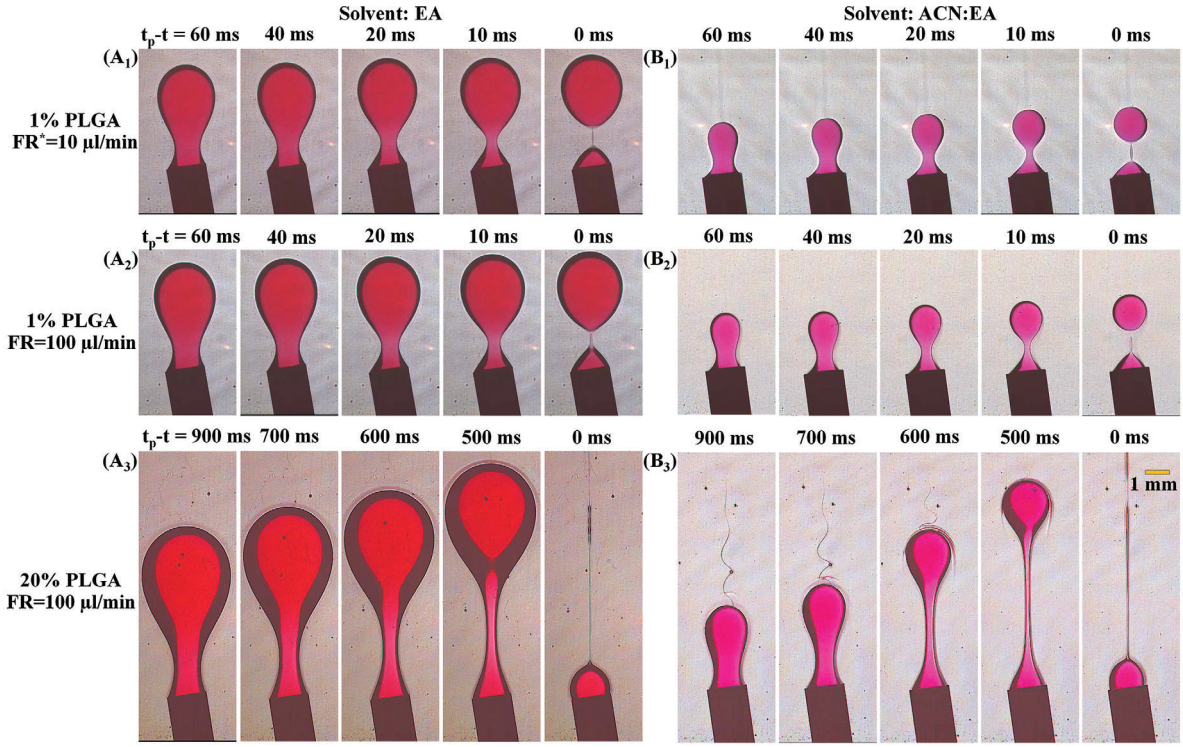

Figure 5. Detachment of oil phase droplets made with PLGA in (A_1-A_3) EA and (B_1-B_3) ACN:EA (1:1-v:v) solvents. The PLGA concentration-oil phase flow rate for (A_1-B_1), (A_2-B_2), and (A_3-B_3) are 1%-10 µL min^{-1}, 1%-100 µL min^{-1}, and 20%-100 µL min^{-1}, respectively. *FR in the figure means the flow rate of the oil phase. The scale bar: 1 mm applies to all the images.

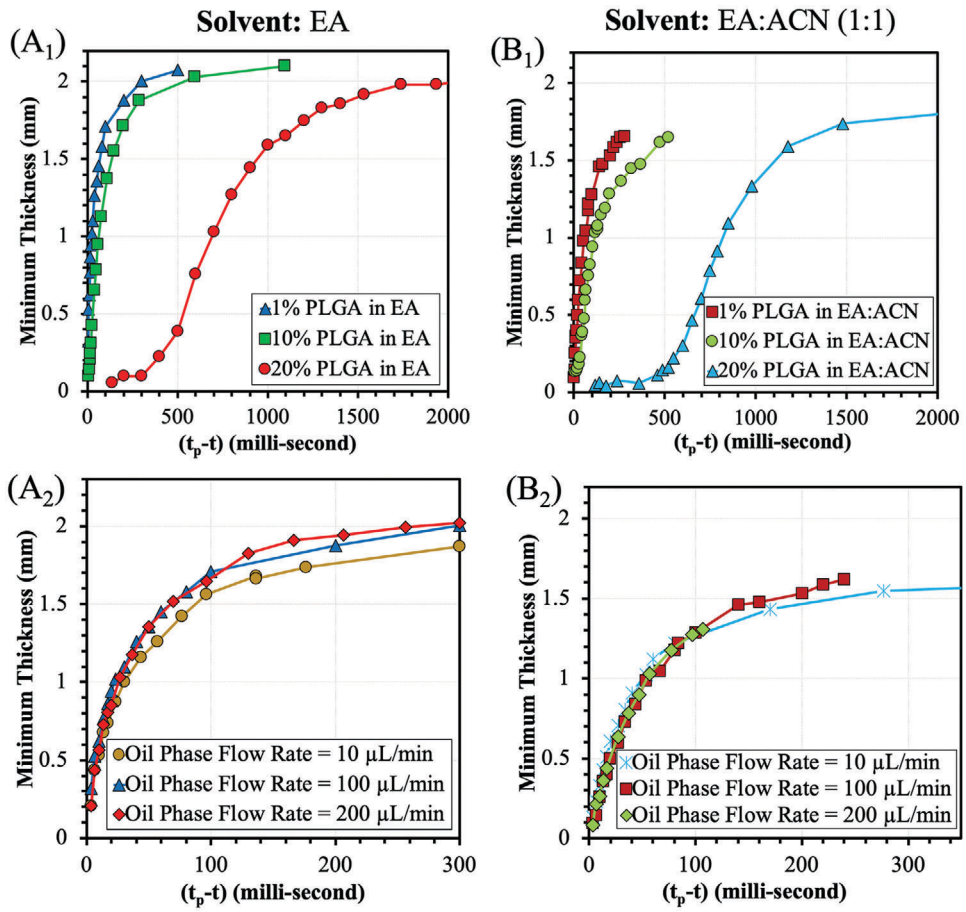

Figure 6. Thinning kinetics of the neck of the oil phase during the droplet formation. The oil phases were made with different PLGA concentrations in (A_1-A_2) EA and (B_1-B_2) ACN:EA (1:1-v:v) solvents. The effects of PLGA concentration and oil phase flow rate are shown in (A_1-B_1) and (A_2-B_2), respectively. In A_1 and B_1, the oil phase flow rate is constant at 100 µL min^{-1}. In A_2 and B_2, the PLGA concentration is constant at 1% (w/w). Data are reported as mean ± SD ($n = 3$).

10%). In contrast, in the higher PLGA concentrations (20% and 30%), the satellites were connected to the strands, and the strands were connected to the droplets (Figure 3,B_3). Additionally, Figure S1 (Supporting Information) demonstrates the images of oil phase droplets made of different concentrations of PLGA in EA. The figure shows a significant increase in the droplet size and strand formation when the PLGA concentration was increased to 20% and 30%. Figure S2 (Supporting Information) shows the phase separation and precipitation of PLGA in the oil phase droplet made of 1% PLGA in EA after 2 h. The phase separation occurred due to the solvent/water exchange process, increased PLGA concentration, and formation of coacervates.[11] Although there is no visible indication of the PLGA precipitation at the surface of the oil phase droplet and skin formation, the generation of the solidified PLGA strands attached to the droplets is clear. This can support the idea of rapid solvent diffusion from the surface of the droplets and skin formation after the oil and water phases contact.

The diameter of the oil phase droplets was measured from different oil phase formulations made with 1–30% PLGA in the organic solvents (**Figure 4**). The droplets made with ACN:EA were smaller than EA due to the higher water solubility of the organic solvent and its faster diffusion from the droplets. Additionally, the viscosity of the oil phase made with EA was higher than ACN:EA due to the higher density of EA compared to ACN:EA (Table 2). This enhanced the viscous force in PLGA-EA droplets, which created more resistance to the oil phase deformation, thus resulting in the formation of droplets with a larger diameter. For the same reason, when the PLGA concentration was increased from 1% to 30%, the diameter of the droplets was increased by 76% and 153% when the organic solvents of ACN:EA and EA were used, respectively. Additionally, Table 2 and Figure 4 demonstrate that the oil phase viscosity is not the only factor in the size of the droplets. For instance, the viscosity of the 30% PLGA in ACN:EA is 2153 mPa s, which is 3.3 times higher than the oil phase viscosity with 20% PLGA in EA (641.8 mPa s). However, the droplet diameter of the oil phase made with 30% PLGA in ACN:EA is 1.65 times smaller than that of 20% PLGA in EA due to the difference in solvent water solubility.

Figure 5 demonstrates the detachment of the oil phases made with PLGA in EA (A_1–A_3) and ACN:EA (1:1-v:v) (B_1–B_3) solvents. The quantitative thinning kinetics of the oil phase droplets is shown in **Figure 6**. In this figure, t_p is the time when pinch-off occurred for each formulation. The minimum thickness of the

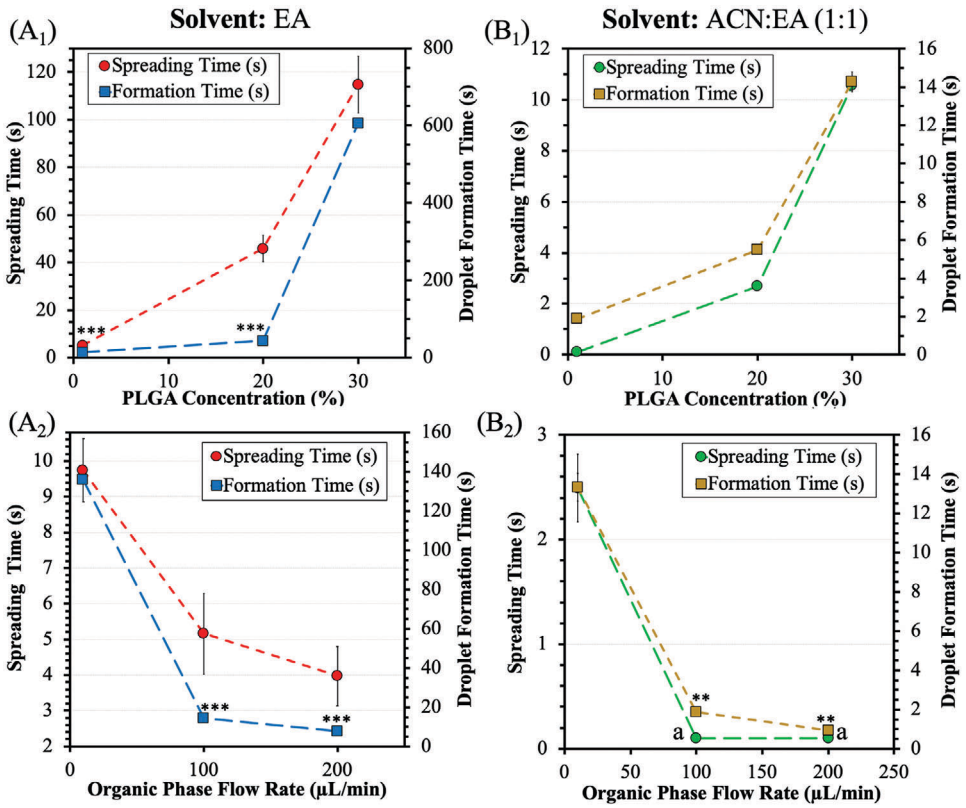

Figure 7. The formation and spreading time (s) of the droplets made with two different solvents (A) EA and (B) ACN:EA. Effects of (A_1 and B_1) PLGA concentration (%) in the oil phase and (A_2 and B_2) oil phase flow rate (µL min^{-1}) on the formation and spreading time (s) of the droplets. The oil phase flow rate was kept constant at 100 µL min^{-1} for (A_1 and B_1), whereas in (A_2 and B_2), the PLGA concentration was 1% (w/w). Data are reported as mean ± SD ($n = 3$, $^{**}p < 0.01$, $^{***}p < 0.001$, *a*: statistically the same).

oil phase was measured as a function of time before the pinch-off time, i.e., $t_p - t$. The first and second rows of Figure 5 compare the effect of the oil phase flow rate when it was increased from 10 to 100 µL min^{-1}, where the PLGA concentration was kept constant at 1%. The figure demonstrates that no significant difference was observed in droplet detachment kinetics when the oil phase was increased from 10 to 100 µL min^{-1}. Figure 6A_1-B_1 supports this observation and indicates that when the flow rate increased further to 200 from 10 µL min^{-1}, the droplet detachment and thinning kinetics remained almost the same.

In the second and third rows of Figure 5, the impact of changing the PLGA concentration on the droplet detachment can be observed. When the PLGA concentration was increased from 1% to 20%, the viscosity of the oil phase increased by 1280 times and 850 times when EA and ACN:EA were used, respectively (Table 2). This significant increase in the viscosity enhanced the viscous force, slowing down the droplet detachment by 15 times. Additionally, the PLGA precipitation became faster when PLGA concentration increased by 20 times. These two factors resulted in the formation of the strands attached to the droplets. Figure 6A_2-B_2 demonstrates that when the PLGA concentration was increased from 1% to 10%, no significant difference was observed in the thinning kinetics. This can be because the viscosity of the oil phase did not change considerably in the PLGA concentration range of 1–10%. However, by increasing the PLGA concentration to 20%, the thinning profile was changed. It was observed that for both of the formulations, i.e., 20% PLGA in EA and 20% PLGA in ACN:EA, in the last 300 ms before the pinch-off, the minimum thickness of the oil phase did not change significantly. This behavior can be because the strand shape organic phase has a higher surface to volume than the sphere shape, resulting in an increased rate of PLGA precipitation/solvent extraction.

Although collimating the light helped improve the contrast and visibility of the diffusion of the ACN from the droplet, the precipitation of PLGA was still not evident. To better understand the impact of parameters on the skin formation of the droplets, the time in which the droplets touched the surface of the water bath until they spread at the surface (due to the change in the surface tension) was measured. **Figure 7** demonstrates the formation and spreading time of the droplets made with the solvents EA and ACN:EA (1:1), PLGA concentrations of 1%, 20%, and 30%, and the oil phase flow rates of 10, 100, and 200 µL min^{-1}. The formation and spreading periods were described in Section 2.5. The formation time was increased when EA was used for all the conditions due to its higher viscosity than ACN:EA (Table 2). Additionally, when the PLGA concentration increased or the oil phase flow rate was reduced, the formation time of the oil phase droplet was increased due to the increased viscous force and reduced inertial force, respectively. For instance, when the PLGA concentration in ACN:EA was increased from 1% to 30%, the formation time of the droplet was increased from 1.89 s to 14.29 s (Figure 7B1).

The spreading time was also affected by the water solubility of the solvent, PLGA concentration, and oil phase flow rate with the same trend as the droplet formation time. For example, when 1% PLGA in ACN:EA was used, and the oil phase flow rate increased from 10 to 100 μL min^{-1}, the droplet formation was reduced from 13.59 s to 1.89 s, and the spreading time was decreased from 2.49 s to 100 ms. This indicates that the droplet formation time can affect the skin formation on the surface of the droplets such that it can affect the spreading time for the droplets made with different formation times.

4. Conclusion

The initial PLGA precipitation to form a skin on the surface of the oil phase droplets over time is a critical aspect in determining the properties of a PLGA-based drug delivery system, and it is often not fully considered. Gaining a more profound knowledge about the time-dependent PLGA precipitation phenomenon at the surface of the oil phase and understanding the effect of parameters on this phenomenon would greatly help control and design the structures of drug/PLGA particles. The current study examined some of the essential steps regarding the precipitation of drug/PLGA microparticles. Additionally, an experiment was designed to generate oil phase droplets with different PLGA concentrations, oil phase flow rates, and organic solvents. The formation of the droplets and PLGA precipitation were studied using a collimated light and a high-speed camera. Although the starting point of PLGA precipitation was not clear with the high-speed camera, our preliminary data suggest that the skin formation can be correlated to the spreading time of the oil phase droplet at the surface of the water phase bath.

Supporting Information

Supporting Information is available from the Wiley Online Library or from the author.

Acknowledgements

This study was supported by UG3 DA048774 from the National Institute on Drug Abuse (NIDA) and the Ralph W. and Grace M. Showalter Research Trust Fund.

Conflict of Interest

The authors declare no conflict of interest.

Data Availability Statement

Research data are not shared.

Keywords

droplet formation, PLGA microparticles, precipitation, seed emulsion, skin formation, solvent diffusion

Received: July 16, 2021
Revised: September 13, 2021
Published online:

[1] M. Vert, *Biomacromolecules* **2005**, *6*, 538.
[2] J. Nicolas, S. Mura, D. Brambilla, N. Mackiewicz, P. Couvreur, *Chem. Soc. Rev.* **2013**, *42*, 1147.
[3] X. Liang, J. Gao, W. Xu, X. Wang, Y. Shen, J. Tang, S. Cui, X. Yang, Q. Liu, L. Yu, J. Ding, *Biofabrication* **2019**, *11*, 035009.
[4] B. Li, Z. Xie, Q. Wang, X. Chen, Q. Liu, W. Wang, Y. Shen, J. Liu, A. Li, Y. Li, G. Zhang, J. Liu, D. Zhang, C. Liu, S. Wang, Y. Xie, Z. Zhang, J. Ding, *Biomaterials* **2021**, *274*, 120851.
[5] H. K. Makadia, S. J. Siegel, *Polymers* **2011**, *3*, 1377.
[6] L. Yu, J. Ding, *Chem. Soc. Rev.* **2008**, *37*, 1473.
[7] T. Ci, L. Chen, L. Yu, J. Ding, *Sci. Rep.* **2014**, *4*, 5473.
[8] Z. Pan, P. Duan, X. Liu, H. Wang, L. Cao, Y. He, J. Dong, J. Ding, *Regener. Biomater.* **2015**, *2*, 9.
[9] D. Cao, X. Chen, F. Cao, W. Guo, J. Tang, C. Cai, S. Cui, X. Yang, L. Yu, Y. Su, J. Ding, *Adv. Funct. Mater.* **2021**, *31*, 2100349.
[10] F. Sharifi, Y. J. Meqbil, A. Otte, A. M. Gutridge, A. T. Blaine, R. M. van Rijn, K. Park, *Pharm. Res.* **2021**, *38*, 1221.
[11] K. Park, A. Otte, F. Sharifi, J. Garner, S. Skidmore, H. Park, Y. K. Jhon, B. Qin, Y. Wang, *J. Controlled Release* **2021**, *329*, 1150.
[12] L. Wu, J. Ding, *Biomaterials.* **2004**, *25*, 5821.
[13] Z. Pan, J. Ding, *Interface Focus* **2012**, *2*, 366.
[14] P. D. Graham, K. J. Brodbeck, A. J. McHugh, *J. Controlled Release* **1999**, *58*, 233.
[15] A. J. McHugh, *J. Controlled Release* **2005**, *109*, 211.
[16] K. Park, S. Skidmore, J. Hadar, J. Garner, H. Park, A. Otte, B. K. Soh, G. Yoon, D. Yu, Y. Yun, B. K. Lee, X. Jiang, Y. Wang, *J. Controlled Release* **2019**, *304*, 125.
[17] L. Yu, Z. Zhang, H. Zhang, J. Ding, *Biomacromolecules* **2010**, *11*, 2169.
[18] J. Li, R. M. Stayshich, T. Y. Meyer, *J. Am. Chem. Soc.* **2011**, *133*, 6910.
[19] Y. Wang, B. Qin, G. Xia, S. H. Choi, *AAPS J.* **2021**, *23*, 92.
[20] J. Lunt, *Polym. Degrad. Stab.* **1998**, *59*, 145.
[21] H. Fukuzaki, M. Yoshida, M. Asano, M. Kumakura, *Eur. Polym. J.* **1989**, *25*, 1019.
[22] D. K. Gilding, A. M. Reed, *Polymer* **1979**, *20*, 1459.
[23] D. Bendix, *Polym. Degrad. Stab.* **1998**, *59*, 129.
[24] C. Jérôme, P. Lecomte, *Adv. Drug Delivery Rev.* **2008**, *60*, 1056.
[25] O. Dechy-Cabaret, B. Martin-Vaca, D. Bourissou, *Chem. Rev.* **2004**, *104*, 6147.
[26] W. Rao, C. Cai, J. Tang, Y. Wei, C. Gao, L. Yu, J. Ding, *Chin. J. Chem.* **2021**, *39*, 1965.
[27] L. Yu, H. Zhang, J. Ding, *Angew. Chem., Int. Ed. Engl.* **2006**, *45*, 2232.
[28] L. Yu, G. Chang, H. Zhang, J. Ding, *J. Polym. Sci., Part A: Polym. Chem.* **2007**, *45*, 1122.
[29] G. Chang, L. Yu, Z. Yang, J. Ding, *Polymer* **2009**, *50*, 6111.
[30] M. J. Blanco-Prıéto, M. A. Campanero, K. Besseghir, F. Heimgatner, B. Gander, *J. Controlled Release* **2004**, *96*, 437.
[31] M. A. Tracy, K. L. Ward, L. Firouzabadian, Y. Wang, N. Dong, R. Qian, Y. Zhang, *Biomaterials* **1999**, *20*, 1057.
[32] A. M. Sophocleous, K.-G. H. Desai, J. M. Mazzara, L. Tong, J.-X. Cheng, K. F. Olsen, S. P. Schwendeman, *J. Controlled Release* **2013**, *172*, 662.
[33] J. Garner, S. Skidmore, H. Park, K. Park, S. Choi, Y. Wang, *J. Pharm. Sci.* **2018**, *107*, 353.
[34] J. V. Andhariya, J. Shen, Y. Wang, S. Choi, D. J. Burgess, *Int. J. Pharm.* **2019**, *566*, 532.
[35] R. Jeyanthi, R. C. Mehta, B. C. Thanoo, P. P. Deluca, *J. Microencapsulation* **1997**, *14*, 163.
[36] F. Sharifi, A. Otte, G. Yoon, K. Park, *J. Controlled Release* **2020**, *325*, 347.
[37] C. Cohen, G. B. Tanny, S. Prager, *J. Polym. Sci., Part A: Polym. Chem* **1979**, *17*, 477.
[38] T.-H. Young, L.-W. Chen, *J. Membr. Sci.* **1991**, *59*, 169.
[39] C. A. Smolders, A. J. Reuvers, R. M. Boom, I. M. Wienk, *J. Membr. Sci.* **1992**, *73*, 259.

[40] M. A. Frommer, R. M. Messalem, *Ind. Eng. Chem. Prod. Res. Dev.* **1973**, *12*, 328.
[41] H. Strathmann, K. Kock, P. Amar, R. W. Baker, *Desalination* **1975**, *16*, 179.
[42] Y.-Y. Yang, H.-H. Chia, T.-S. Chung, *J. Controlled Release* **2000**, *69*, 81.
[43] A. Budhian, S. J. Siegel, K. I. Winey, *Int. J. Pharm.* **2008**, *346*, 151.
[44] L. Mu, S. S. Feng, *J. Controlled Release* **2003**, *86*, 33.
[45] S. Takada, Y. Yamagata, M. Misaki, K. Taira, T. Kurokawa, *J. Controlled Release* **2003**, *88*, 229.
[46] D. T. O'Hagan, H. Jeffery, S. S. Davis, *Int. J. Pharm.* **1994**, *103*, 37.
[47] W. K. Lee, J. Y. Park, E. H. Yang, H. Suh, S. H. Kim, D. S. Chung, K. Choi, C. W. Yang, J. S. Park, *J. Controlled Release* **2002**, *84*, 115.
[48] M. Ochi, B. Wan, Q. Bao, D. J. Burgess, *Int. J. Pharm.* **2021**, *599*, 120450.
[49] Y. Y. Yang, T. S. Chung, N. P. Ng, *Biomaterials* **2001**, *22*, 231.
[50] S. Cohen, T. Yoshioka, M. Lucarelli, L. H. Hwang, R. Langer, *Pharm. Res.* **1991**, *8*, 713.
[51] H. Sah, R. Toddywala, Y. W. Chien, *J. Controlled Release* **1994**, *30*, 201.
[52] M. S. Hora, R. K. Rana, J. H. Nunberg, T. R. Tice, R. M. Gilley, M. E. Hudson, *Pharm. Res.* **1990**, *7*, 1190.
[53] R. C. Mehta, B. C. Thanoo, P. P. Deluca, *J. Controlled Release* **1996**, *41*, 249.
[54] F. Sharifi, A. Otte, G. Yoon, K. Park, *J. Controlled Release* **2020**, *325*, 347.
[55] Y. Y. Hsu, T. Hao, M. L. Hedley, *J. Drug Targeting* **1999**, *7*, 313.
[56] C. Martin-Sabroso, A. I. Fraguas-Sanchez, J. Aparicio-Blanco, M. F. Cano-Abad, A. I. Torres-Suarez, *Int. J. Pharm.* **2015**, *480*, 27.
[57] D. Klose, F. Siepmann, K. Elkharraz, S. Krenzlin, J. Siepmann, *Int. J. Pharm.* **2006**, *314*, 198.
[58] G. Acharya, C. S. Shin, K. Vedantham, M. McDermott, T. Rish, K. Hansen, Y. Fu, K. Park, *J. Controlled Release* **2010**, *146*, 201.
[59] W. Chen, A. Palazzo, W. E. Hennink, R. J. Kok, *Mol. Pharmaceutics* **2017**, *14*, 459.
[60] X. Li, X. Deng, M. Yuan, C. Xiong, Z. Huang, Y. Zhang, W. Jia, *Int. J. Pharm.* **1999**, *178*, 245.
[61] R. Jeyanthi, B. C. Thanoo, R. C. Metha, P. P. Deluca, *J. Controlled Release* **1996**, *38*, 235.
[62] W. Lan, S. Li, G. Luo, *Chem. Eng. Sci.* **2015**, *134*, 76.
[63] R. Tahery, H. Modarress, J. Satherley, *J. Chem. Eng. Data* **2006**, *51*, 1039.
[64] I. M. Hauner, A. Deblais, J. K. Beattie, H. Kellay, D. Bonn, *J. Phys. Chem. Lett.* **2017**, *8*, 1599.
[65] J. Eggers, *Rev. Mod. Phys.* **1997**, *69*, 865.
[66] M. Tjahjadi, H. A. Stone, J. M. Ottino, *J. Fluid Mech.* **1992**, *243*, 297.